Eur. Phys. J. C 49, 359–364 (2007)
DOI 10.1140/epjc/s10052-006-0124-3

THE EUROPEAN PHYSICAL JOURNAL C

Regular Article – Experimental Physics

Open heavy flavor production from single muons in PHENIX at RHIC

D.J. Kim[a] for the PHENIX Collaboration

IPAP, Yonsei University, Seoul, 120-749, South Korea

Received: 3 August 2006 /
Published online: 27 October 2006 –

Abstract. The PHENIX experiment has studied open heavy flavor production in $\sqrt{s_{NN}} = 200$ GeV $p+p$ and $d+\mathrm{Au}$ collisions using the semi-leptonic decay into single muons. The results from these measurements and the details of the analysis technique are presented. The results from $p+p$ collisions obtained at mid-rapidity are compared to perturbative QCD calculations. The production of light mesons is the major background source for the open flavor measurement using muons. The nuclear modification factor for light mesons were measured in $\mathrm{Cu}+\mathrm{Cu}$ collisions at $\sqrt{s_{NN}} = 200$ GeV is presented.

1 Introduction

The interaction of heavy quarks with the hot dense matter created in heavy ion collisions at RHIC, is a very important probe to understand the properties of the produced medium. It has been experimentally measured that the neutral pions and charged hadrons are strongly suppressed at high transverse momentum in high energy $\mathrm{Au}+\mathrm{Au}$ collisions [1,2]. The suppression, which is absent in $d+\mathrm{Au}$ collisions at mid-rapidity, implies that hard scattered partons traveling through the medium created in such collisions experience considerable energy loss. The same effect for heavy quarks is predicted to be smaller than for the light quarks due to a suppression of the phase space for gluon radiation for large masses of the quarks (the so called "dead cone" effect [3]). Due to the interactions of heavy quarks with the medium, the heavy flavor particles are expected to exhibit non-zero elliptic flow v_2 [4]. The strength of the heavy quark flow in combination with the degree of suppression of heavy flavor hadrons provide crucial information on the the transport properties of the medium and the energy loss mechanism [5].

Measurements of heavy quark production in proton–proton ($p+p$) interactions at collider energies serve as important tests for perturbative quantum chromodynamics (pQCD). Bottom production at FNAL ($\sqrt{s} = 1.8$ and 1.96 GeV/c) [6,7] is reasonably well described by a recent fixed order next-to-leading logarithm (FONLL) calculation [8,9]. Charm production at FNAL, which has only been measured at relatively high p_{T} (> 5 GeV/c), is about 50% higher than the FONLL prediction [10]. However, theoretical and experimental uncertainties are large, such that significant disagreement between theory and data cannot be claimed.

Both PHENIX [21–26] and STAR [28] have made statistical measurements of charm production via single-electron spectra. STAR has also made a direct measurement of charm production through reconstruction of hadronic decay modes of D mesons [28]. In $p+p$ collisions PHENIX finds $\mathrm{d}\sigma_{c\bar{c}}/\mathrm{d}y|_{y=0} = 0.20 \pm 0.03(\mathrm{stat.}) \pm 0.11(\mathrm{syst.})$. STAR finds a somewhat higher central value, $\mathrm{d}\sigma_{c\bar{c}}/\mathrm{d}y|_{y=0} = 0.30 \pm 0.04(\mathrm{stat.}) \pm 0.09(\mathrm{syst.})$, but the two measurements are consistent within the stated errors. Both measurements are noticeably higher than PYTHIA [29] and FONLL [11]. Quantitative disagreement cannot be established with current experimental and theoretical errors.

During the 2004 run of RHIC, PHENIX collected a high statistics $\mathrm{Au}+\mathrm{Au}$ data sample and a minimum bias sample of 460×10^6 events was analyzed using the beam–beam counter (BBC) as a trigger source. A factor of 100 statistical improvement compared to the previously published data [22] was achieved due to the larger integrated luminosity, a factor of two increase in acceptance and a reduction of the photonic background by removing of material in the detector central region. For the $p+p$ results, the low p_{T} part come from the 9.8×10^6 minimum bias events while the high p_{T} part come from the events firing the level-1 electron trigger (ERT) corresponding effectively to 2.3×10^9 minimum bias events. Comparing to the previously published results $p+p$ results [23], the luminosity is increased five times and electron acceptance improved by a factor of four. The total material budget of the PHENIX detector corresponded to $X \approx 0.7\%$ X_0 radiation length from the beam pipe (0.4%) and air (0.3%) which give us the large signal to noise significantly, shown in Fig. 1.

[a] e-mail: djkim@bnl.gov, present address: Department of Physics, University of Jyvaslyla, P.O. Box 35, 40014 Jyvaskyla, Finland

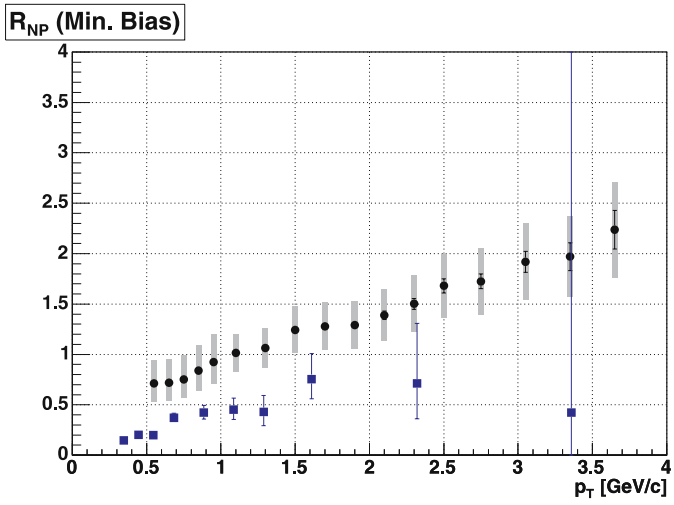

Fig. 1. Ratio of non-photonic to photonic electrons from Au + Au collisions in run 4 (*black*) and run 2 (*blue*) converter runs

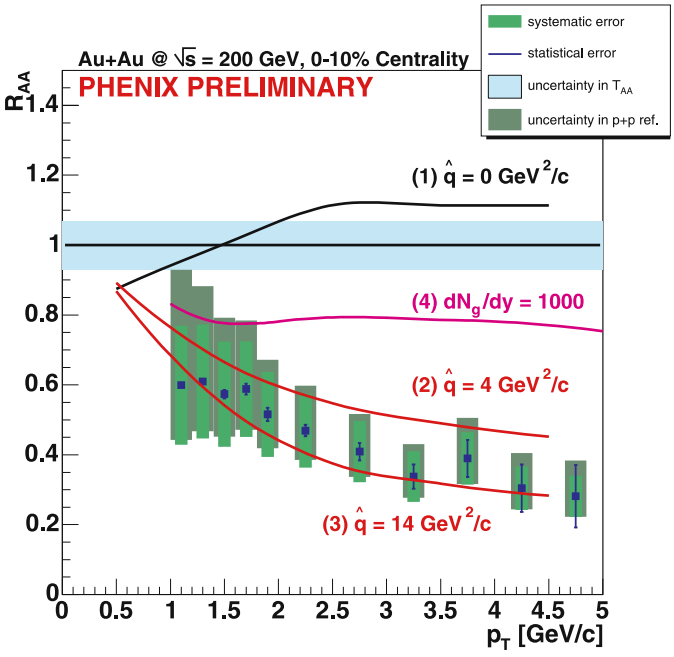

Fig. 2. "Non-photonic" electron for 0–10% centrality bin compared with theoretical predictions. Theory curves (1)–(3) from [36], (4) from [37]

Strong suppression increasing with centrality was observed in the production of "non-photonic" electrons in Au + Au collisions. The results on the nuclear modification factor R_{AA}, shown in Fig. 2 may provide a significant constraint on the theoretical description of the heavy quark energy loss mechanisms. While most energy loss calculations consider only radiative energy loss [13–17], recent analyses suggest that collisional energy loss could contribute significantly in the currently accessible momentum range [18, 19] – particularly for heavy quarks [5, 20]. Even though currently the experimental statistical errors are large, there are rooms for improvements on the recent energy loss calculation [5, 20].

Until now, open charm measurements at RHIC have been limited to mid-rapidity. Measurements at forward rapidity are interesting for a variety of reasons. First is the need to constrain theoretical calculations over a wide kinematic range. This is demonstrated by the theoretical improvements motivated [12] by the observation of an increasing discrepancy between theory and the D0 measurement of bottom production at large rapidity ($\sqrt{s} = 1.8\,\mathrm{TeV}$, $p_\mathrm{T} > 5\,\mathrm{GeV}/c$, $2.4 < y_\mu < 3.2$), as deduced from the production of hard muons [6]. Second, significant cold nuclear effects have been seen in RHIC collisions at forward rapidity. PHENIX [32] and BRAHMS [30, 31] have both measured light hadron production in $d+\mathrm{Au}$ collisions at forward rapidity and have found significant deviations from $R_{d\mathrm{Au}} = 1$. It will be interesting to see whether charm production follows a similar pattern. Finally, open charm production at forward rapidity needs to be understood to fully interpret PHENIX J/ψ measurements at forward rapidity [33–35].

In this paper we report on the PHENIX measurement of inclusive muon candidates at forward rapidity , at $\sqrt{s} = 200\,\mathrm{GeV}$ $p+p$, $d+\mathrm{Au}$ and $\mathrm{Cu}+\mathrm{Cu}$ collisions with the detail analysis technique. The prompt muon yield is statistically extracted by subtracting contributions from the muon decay of light mesons (π's and K's) and the penetration of hadrons through the muon arm absorbers.

2 The PHENIX Experiment

The PHENIX experiment, shown in Fig. 3, is a large multipurpose set of detectors optimized for the measurement of relatively rare electromagnetic probes (photons, muons, and electrons) of proton spin structure and of the hot dense matter created in ultrarelativistic heavy ion collisions. The data acquisition system and multilevel triggers are designed to handle the bandwidth extremes represented by $p+p$ collisions (relatively small events at large rates) and Au + Au collisions (large events at relatively low rates) with little or no deadtime. Event characterization devices, such as the beam–beam counters used in this analysis, provide information on the collision vertex position, start time, and centrality. The two muon arms cover $1.2 < |\eta| < 2.4$ in pseudorapidity and $\delta\varphi = 2\pi$ in azimuth. The two central arms cover $|\eta| < 0.35$ and $\delta\varphi = \pi/2$.

The muon arms are coaxial with the beam on opposite sides of the collision vertex. By convention the arm on the South (North) end of the interaction region is assigned negative (positive) z coordinates and rapidity. Each muon arm is comprised of a muon tracker (MuTR) and a muon identifier (MuID). The MuTR measures particle momenta with a resolution of $\sigma_p/p \approx 5\%$ over the analyzed kinematic range. The MuID allows coarse resolution track reconstruction through five layers of chambers interleaved with steel absorbers.

Each MuTR arm consists of three stations of cathode strip chambers installed in an eight-sided conical magnet.

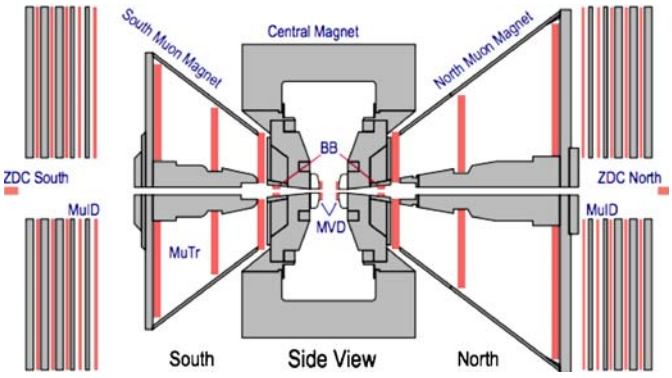

Fig. 3. PHENIX detector configuration for run 4

The radial magnetic field ($\int \mathbf{B}\,\mathrm{d}\mathbf{l} = 0.72\,\mathrm{T\,m}$) bends particles in the azimuthal direction. Each station occupies a plane perpendicular to the beam axis and consists of multiple ionization gaps which have their charge imaged on two cathode strip planes oriented with a small stereo angle to provide two-dimensional information. An ionizing particle typically fires three adjacent strips in each orientation. A fit to the charge distribution on adjacent strips provides a position measurement with a resolution of $\sigma \approx 100\,\mu$m in the bend direction. The MuTR occupancy is greatly reduced by front absorber layers: 20 cm of copper plus 60 cm of iron. The nominal nuclear interaction lengths of iron and copper are $\lambda_{\mathrm{I}}^{\mathrm{Fe}} = 16.7\,\mathrm{cm}$ and $\lambda_{\mathrm{I}}^{\mathrm{Cu}} = 15.3\,\mathrm{cm}$. Therefore the pre-MuTR absorber presents a total thickness of $4.9/\cos\theta\lambda_{\mathrm{I}}$, where θ is the polar angle of a particle's trajectory.

Each MuID arm consists of five steel absorber plates, the gaps of which are filled with Iarocci tubes operated in proportional mode. Gaps are labeled 0–4 proceeding downstream from the collision point. Digital readout of the Iarocci tube anode signals provides coarse one-dimensional hit position information ($\sigma = 9\,\mathrm{cm}/\sqrt{12} = 2.6\,\mathrm{cm}$). The tubes in each gap are housed in six individual panels, each of which contains two layers of tubes (horizontally and vertically oriented), thus providing two dimensional information. The first MuID absorber plate (thickness = 20 cm – south; 30 cm – north) also serves as the return yoke of the MuTR magnet. Successive plates (identical for two arms) are 10, 10, 20 and 20 cm thick, thus totaling $4.8/\cos\theta\lambda_{\mathrm{I}}$ ($5.4/\cos\theta\lambda_{\mathrm{I}}$) for the south (north) arm. Due to ionization energy loss a particle must have $p[\mathrm{GeV}/c] > 2.31/\cos\theta$ ($2.45/\cos\theta$) in order to penetrate to the most downstream MuID gap (gap 4) of the south (north) arm.

3 How to extract muons from charm decay

Inclusive muon candidates, N_{I}, are those particles which are successfully reconstructed to the last MuID gap (gap 4). These consist of four components: 1) "decay muons", N_{D}, which result from the decay of light hadrons (π and K mesons) before reaching the MuTR, 2) "punchthrough hadrons", N_{P}, which penetrate the entire detector and are thus misidentified as muons 3) "background tracks", N_{B}, which in $p+p$ collisions are dominated by hadrons which decay into a muon after reaching the MuTR, and 4) "prompt muons", N_{μ}, which are primarily due to the decay of heavy flavor mesons. Figure 4 shows a schematic depiction of the relative yield per event of these different contributions as a function of flightpath into the muon arms. The number of hadrons is large and essentially independent of flightpath until the first absorber layer is reached. In each absorber layer these hadrons undergo strong interactions with a probability $1-\exp(-L/\lambda)$, where L is the length of absorber material traversed, and λ is the species and p_{T}-dependent nuclear interaction length. Such interacting hadrons are effectively eliminated as possible muon candidates. However, a small fraction of hadrons penetrate the entire absorber thickness without a strong interation. These punchthrough hadrons are indistinguishable from a prompt muon. The decay lengths for π's ($c\tau = 780\,\mathrm{cm}$) and K's ($c\tau = 371\,\mathrm{cm}$) are long compared to the flightpath from the vertex to the absorber. Therefore, the fraction of decay muons from these sources is relatively small, but increases linearly with the flightpath until the first absorber layer is reached. A hadron which decays prior to the pre-MuTR absorber into a muon that is inside the detector acceptance is indistinguishable from a prompt muon. After the first absorber layer the number of decay muons remains relatively constant since the parent hadrons are exponentially absorbed. The small contribution from background tracks is not shown. Prompt muons (from *e.g.* decay of open heavy flavor hadrons, quarkonia or light vector mesons, and Drell-Yan) originate indistinguishably close to the collision vertex. Thus, their yield is independent of flightpath. Since inclusive muon candidates, by definition, penetrate to MuID gap 4, we are measuring the combined yield at $z \approx 870\,\mathrm{cm}$. Figure 5 shows a sample distribution of the inclusive muon candidate yield as a function of collision vertex (z_{vtx}), and its decomposition into the four different contributions. The yield of decay muons is seen to have a linear dependence that is set to 0 at $z_{\mathrm{vtx}} = z_{\mathrm{abs}} - \lambda$. Here $z_{\mathrm{abs}} = -40\,\mathrm{cm}$ is the upstream face the pre-MuTR absorber (indicated by the thick solid

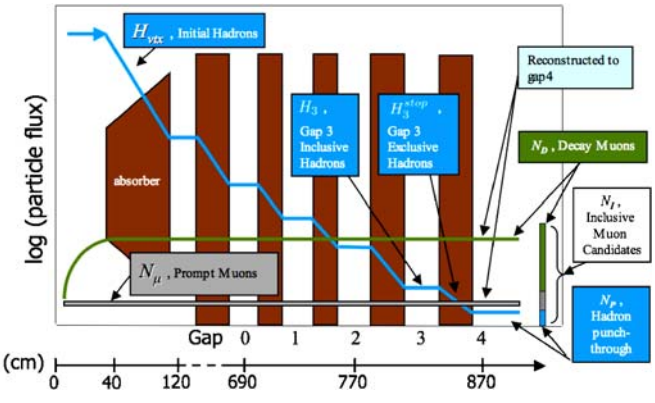

Fig. 4. Schematic depiction of the relative flux of muon candidates as a function of flightpath into the muon arm absorber (the event vertex is at $z_{\mathrm{vtx}} = 0$). See text for details

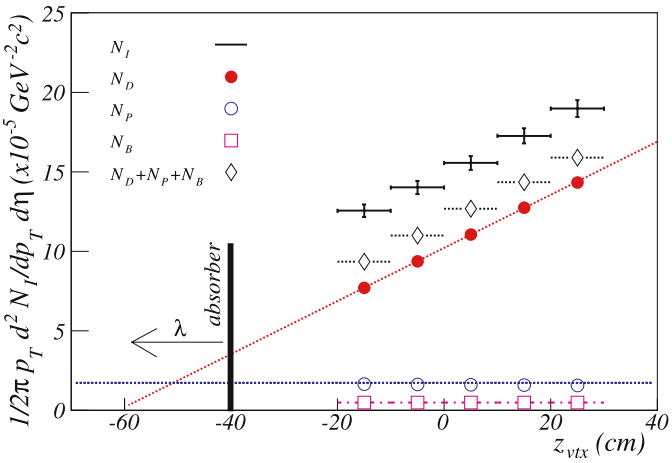

Fig. 5. Sample $z_{\rm vtx}$ distribution of different sources of inclusive muon candidates. *Crosses* show inclusive muon candidates, *filled circles* show decay muons, *open circles* show punchthrough hadrons, *open squares* show background tracks, and *open diamonds* show the sum of these three hadronic sources. The prompt muon yield is obtained from the difference between the yield of inclusive muon candidates and the yield of hadronic sources

line), and λ is the species and $p_{\rm T}$-dependent nuclear interaction length. Muons originating from meson decays downstream of this location have no $z_{\rm vtx}$ dependence, and form the majority of the small contribution from background tracks. The yield of punchthrough hadrons and prompt muons also have no $z_{\rm vtx}$ dependence. Note that the ratio of different contributions to the inclusive muon candidate spectrum is $p_{\rm T}$ dependent.

In order to extract the cross section for charm production we first need to determine the yield of prompt muons, $N_\mu(p_{\rm T})$, the amount beyond that due to light hadrons and fake backgrounds. We obtain the yield of inclusive muon candidates vs. $p_{\rm T}$ and $z_{\rm vtx}$, corrected for acceptance and efficiency: $N_{\rm I}(p_{\rm T}, z_{\rm vtx})$. We use hadrons which stop in MuID gap 3 , together with simulations of hadron penetration in the MuID absorber, to obtain the yield of punchthrough hadrons in MuID gap 4: $N_{\rm P}(p_{\rm T}, z_{\rm vtx})$. The yield of fake tracks, $N_{\rm B}(p_{\rm T}, z_{\rm vtx})$, determined from simulations , is found to be small.

The yield of prompt muons is determined by subtracting the contributions from hadrons and fake backgrounds and averaging over $z_{\rm vtx}$ bins:

$$N_\mu(p_{\rm T}) = \frac{1}{N_{\rm vtx}} \sum_{j=1}^{N_{\rm vtx}} N_{\rm I}\left(p_{\rm T}, z^j_{\rm vtx}\right) - N_{\rm D}\left(p_{\rm T}, z^j_{\rm vtx}\right) - N_{\rm P}\left(p_{\rm T}, z^j_{\rm vtx}\right) - N_{\rm B}\left(p_{\rm T}, z^j_{\rm vtx}\right),$$

where $1/2\pi p_{\rm T}\,{\rm d}p_{\rm T}\,{\rm d}\eta$ is implicit in all terms of the equation. We convert this into a cross section via

$$\frac{{\rm d}^2\sigma_\mu(p_{\rm T})}{2\pi p_{\rm T}\,{\rm d}p_{\rm T}\,{\rm d}y} = \frac{\sigma^{pp}_{\rm BBC}}{\varepsilon^{c,\bar{c}\to\mu}_{\rm BBC}} \frac{{\rm d}^2N_\mu(p_{\rm T})}{2\pi p_{\rm T}\,{\rm d}p_{\rm T}\,{\rm d}\eta}. \quad (1)$$

Here $\sigma_{\rm BBC}$ is the cross section of the BBC trigger for $p+p$ interactions and $\varepsilon^{c,\bar{c}\to\mu}_{\rm BBC}$ is the efficiency of the BBC trigger for events in which a charm quark is created and decays into a muon. Substituting $\eta \to y$ introduces negligible error due to the small mass of the muon. Systematic errors are determined for each component and combined into a term that applies to the overall normalization and a term that applies to the $p_{\rm T}$ dependence of the spectrum.

4 Results

4.1 $p+p$ collisions

The invariant differential cross section of excess leptons are shown with PYTHIA and fixed-order plus next-to-leading-log (FONLL [44]) calculation in Figs. 6 and 7. The PYTHIA and FONLL calculation includes heavy quark production via LO (leading order)/NLO (next to leading order) pQCD calculation and its subsequent decay into leptons. The calculations underpredict the data at high $p_{\rm T}$ within marginal uncertainties.

The plot for prompt muons includes fit of electron spectra, and shows the excess lepton spectra at $y = 0$ and at $y = 1.65$ are similar over the observed $p_{\rm T}$ range. The underprediction of the data by the calculation at forward

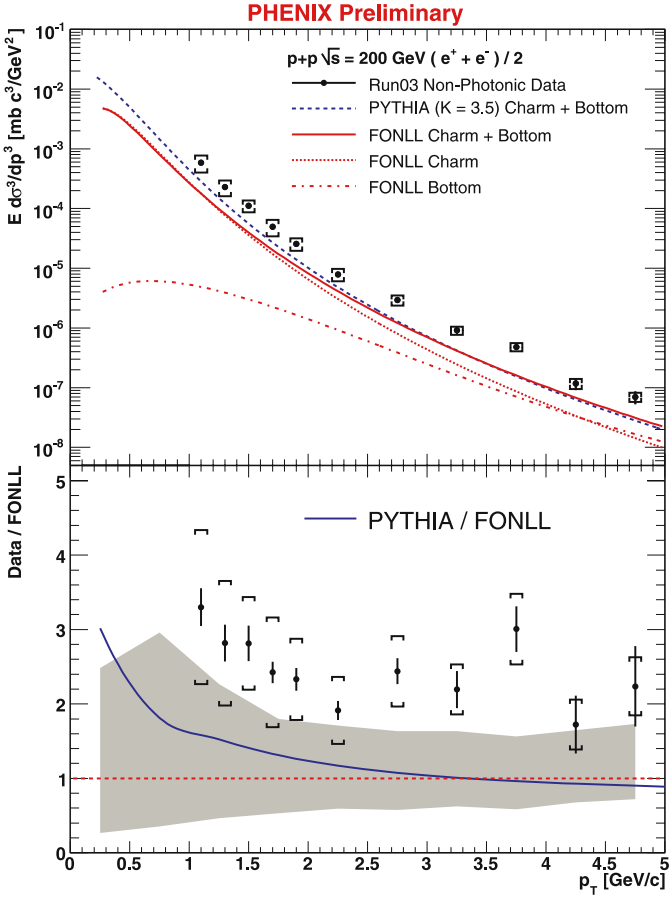

Fig. 6. The non-photonic single electron spectra from the $p+p$ collisions at $\sqrt{s_{NN}} = 200$ GeV and comparison with the FONLL prediction [44]

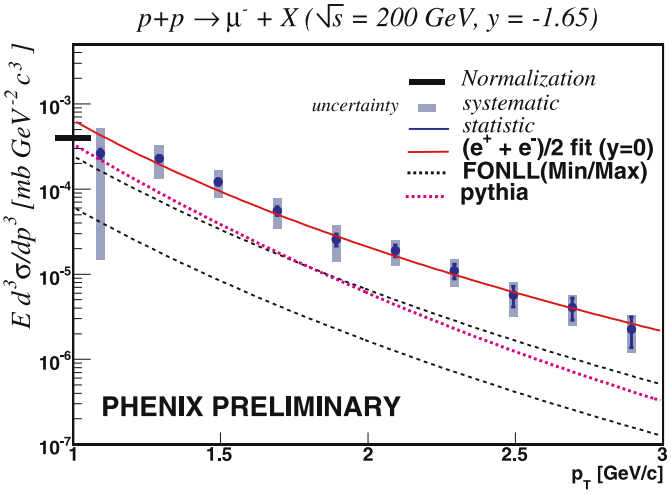

Fig. 7. The prompt muon spectra is shown with the non-photonic single electron spectra from the $p+p$ collisions at $\sqrt{s_{NN}} = 200$ GeV, compared with PYTHIA and FONLL calculation [44]

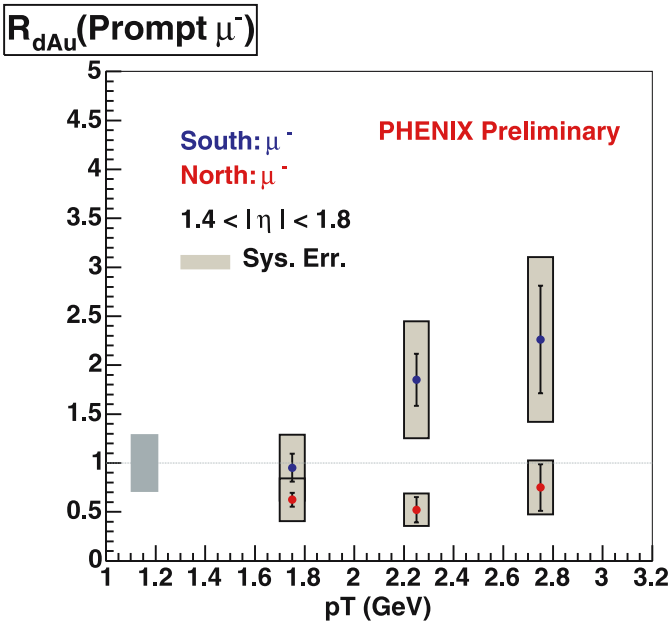

Fig. 8. $R_{d\mathrm{Au}}$ for the prompt muons, $d+$Au collisions at $\sqrt{s_{NN}} = 200$ GeV

rapidity is even stronger than the one at mid-rapidity due to the stronger rapidity dependence of production in the calculations.

4.2 $d+$ Au collisions

The non-photonic electron production in $d+$Au collisions in the mid-rapidity exhibits scaling with N_{coll} indicating point-like interactions [24].

Figure 8 shows nuclear modification factor defined as

$$R_{d\mathrm{Au}}(p_{\mathrm{T}},\eta) \equiv \left(\frac{1}{2\cdot 197}\frac{\mathrm{d}^2\sigma^{d+\mathrm{Au}\to\mu+X}}{\mathrm{d}p_{\mathrm{T}}\,\mathrm{d}\eta}\right)\Big/\left(\frac{\mathrm{d}^2\sigma^{p+p\to\mu+X}}{\mathrm{d}p_{\mathrm{T}}\,\mathrm{d}\eta}\right) \quad (2)$$

for the prompt muons.

$R_{d\mathrm{Au}}$ for deutron-going (forward)/Au-going (backward) side are smaller (suppression)/larger (enhancement) than 1 (N_{coll} scaling) within large uncertainties.

4.3 Cu$+$Cu collisions

The measurement of open charm production in various collision species at different energies is important to study the properties of matter formed in the early stage of relativistic heavy ion collisions, especially to understand charm energy loss. The RHIC facility provided Cu$+$Cu collisions at $\sqrt{s_{NN}} = 200$, 62 and 22 GeV in 2005. This lighter colliding system compared with Au$+$Au can give much better N_{part} and N_{coll} precision in the lower N_{part} region, and the comparison between two different colliding energies may give us a better systematic understanding of charm production.

The nuclear modication factor R_{AA} of the muons from light meson decay in minimum bias collisions shown in Fig. 9 has been measured with the limited statistics at this moment (7% out of the total 3 nb^{-1}) in Cu$+$Cu collisions at $\sqrt{s} = 200$ GeV, $p+p$ reference is taken from [27]. Within the statistical and systematical errors, the R_{AA} is very close to the measurement in the mid-rapidity [45, 46].

Also the light meson yield as a function of rapidity shown in Fig. 10 has been measured, shows the moderate Gaussian distribution. One of the major 1st background source is measured and the method is well estiblished. With the large set of $p+p$ data from RHIC run 5 (3.8 pb^{-1}) taken during 2004–2005, we will be able to reduce the systematic uncertainty on measuring the 2nd major background in higher transverse momentum, which is described in Sect. 3.

5 Summary

The invariant differential cross section for muon candidate production at forward rapidity ($1.5 \le |\eta| \le 1.8$) has been measured by the PHENIX experiment over the transverse momentum range $1 \le p_{\mathrm{T}} \le 3$ GeV/c in $\sqrt{s} = 200$ GeV $p+p$ collisions at RHIC. After statistically subtracting contributions to the muon candidate yield from light hadrons an excess remains. This excess is attributed to the semileptonic decays of hadrons carrying heavy flavor, *i.e.* charm quarks or, at high p_{T}, bottom quarks. The resulting muon spectrum from heavy flavor decays is compared to PYTHIA and a next-to-leading order perturbative QCD calculation. FONLL, current NLO pQCD calculation (semileptonic decays of charm and bottom hadrons), underpredicts the measured excess for $p+p$ collisions within marginal uncertainties. Efforts to reduce the uncertainties are in progress with the large data set of RHIC run 5. PHENIX measured $R_{d\mathrm{Au}}(p_{\mathrm{T}})$ of the prompt muons and the light mesons at forwasrd/backward rapidities for $d+$

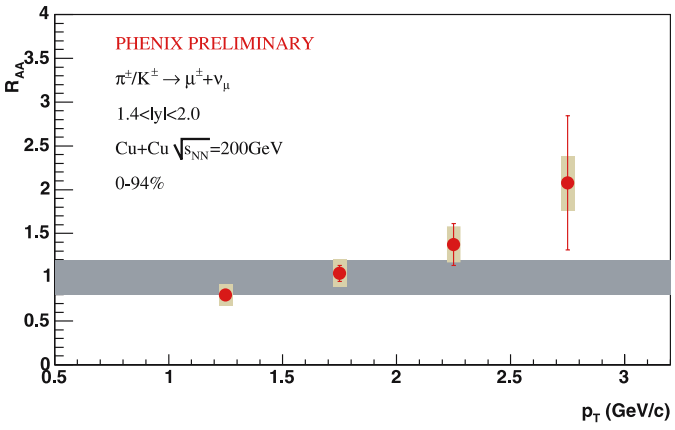

Fig. 9. R_{AA} for the light mesons as a function of p_{T}, Cu + Cu collisions at $\sqrt{s_{NN}} = 200$ GeV

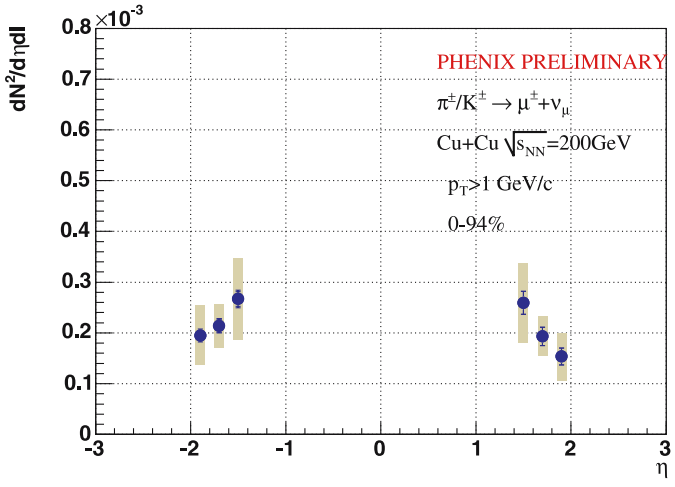

Fig. 10. Rapidity distribution of the light mesons in Cu + Cu collisions at $\sqrt{s_{NN}} = 200$ GeV

Au collisions. Modification of the N_{coll} scaling is seen at forward/backward rapidities within large uncertainties.

The systematic uncertainty in this analysis is dominated by uncertainty on the determination of the fractional contribution of decay muons. This will be improved with higher statistics data set which were taken in 2005. Currently we have measured the light meson spectrum with 7% of Cu + Cu minimum bias collisions at $\sqrt{s} = 200$ GeV which is shown in Sect. 4.3.

References

1. K. Adcox et al., Phys. Rev. Lett. **88**, 022 301 (2002)
2. S.S. Adler et al., Phys. Rev. Lett. **91**, 072 301 (2003)
3. Y.L. Dokshitzer, D.E. Kharzeev, Phys. Lett. B **519**, 199 (2001)
4. S.S. Adler et al., Phys. Rev. Lett. **91**, 182 301 (2003)
5. M.G. Mustafa, Phys. Rev. C **72**, 014 905 (2005) [hep-ph/0412402]
6. B. Abbott et al., Phys. Rev. Lett. **84**, 5478 (2000)
7. D. Acosta et al., Phys. Rev. D **77**, 032 001 (2005)
8. M. Cacciari, hep-ph/0407187 (2004)
9. M. Cacciari, hep-ph/9803400 (1998)
10. D. Acosta et al., Phys. Rev. Lett. **91**, 241 804 (2003)
11. M. Cacciari, P. Nason, R. Vogt, Phys. Rev. Lett. **95**, 122 001 (2005)
12. L. Mangano, J. High Energy Phys. **0407**, 033 (2004)
13. X.-N. Wang, M. Gyulassy, M. Plumer, Phys. Rev. D **51**, 3436 (1995)
14. R. Baier et al., Nucl. Phys. B **483**, 29 (1997) [hep-ph/9607355]
15. B.G. Zakharov, JETP Lett. **65**, 615 (1997) [hep-ph/9704255]
16. M. Gyulassy, P. Levai, I. Vitev, Phys. Rev. Lett. **85**, 5535 (2000)
17. B.G. Zakharov, JETP Lett. **80**, 617 (2004) [hep-ph/0410321]
18. M.H. Thoma, J. Phys. G **26**, 1507 (2000) [hep-ph/0003016]
19. M.G. Mustafa, M.H. Thoma, Acta Phys. Hung. A **22**, 93 (2005) [hep-ph/0311168]
20. G.D. Moore, D. Teaney, Phys. Rev. C **71**, 064 904 (2005) [hep-ph/0412346]
21. S.S. Adler et al., Phys. Rev. Lett. **88**, 192 303 (2002)
22. S.S. Adler et al., Phys. Rev. Lett. **94**, 082 301 (2005)
23. S.S. Adler et al., Phys. Rev. Lett. **96**, 032 001 (2006)
24. PHENIX Collaboration, S. Kelly, J. Phys G **30**, 1189 (2004)
25. S.S. Adler et al., nucl-ex/0510047
26. PHENIX Collaboration, S. Butsyk, nucl-ex/0510010
27. PHENIX Collaboration, Y. Kwon, nucl-ex/0510011
28. STAR Collaboration, J. Bielcik, nucl-ex/0511005
29. T. Sjöstrand et al., hep-ph/0010017
30. I. Arsene et al., Phys. Rev. Lett. **93**, 242 303 (2004)
31. I. Arsene et al., Phys. Rev. Lett. **94**, 032 301 (2005)
32. S.S. Adler et al., Phys. Rev. Lett. **94**, 082 302 (2005)
33. S.S. Adler et al., Phys. Rev. Lett. **92**, 051 802 (2004)
34. S.S. Adler et al., Phys. Rev. Lett. **96**, 012 304 (2006)
35. PHENIX Collaboration, H. Pereira Da Costa, nucl-ex/0510051
36. N. Armesto, S. Dainese, C. Salgado, U. Wiedemann, Phys. Rev. D **71**, 054 027 (2005)
37. M. Djordjevic, M. Gyulassy, S. Wicks, Phys. Rev. Lett. **94**, 112 301 (2005)
38. S.S. Adler et al., Phys. Rev. C **72**, 024 901 (2005)
39. V. Greco, C.M. Ko, R. Rapp, Phys. Lett. B **595**, 202 (2004)
40. J.C. Collins, D.E. Soper, G. Sterman, Nucl. Phys. B **263**, 37 (1986)
41. M.L. Mangano et al., Nucl. Phys. B **405**, 507 (1993)
42. Z. Lin, M. Gyulassy, Phys. Rev. Lett. **77**, 1222 (1996)
43. PHENIX Collaboration, K. Adcox et al., NIM A **499**, 469 (2003)
44. M. Cacciari, P. Nason, R. Vogt, hep-ph/0502203
45. PHENIX Collaboration, M. Konno, nucl-ex/0510022
46. PHENIX Collaboration, M. Shimomura, nucl-ex/0510023